Applied Catalysis B: Environmental 239 (2018) 628–635

Contents lists available at ScienceDirect

Applied Catalysis B: Environmental

journal homepage: www.elsevier.com/locate/apcatb

Catalytic HCl oxidation reaction: Stabilizing effect of Zr-doping on CeO_2 nano-rods

Chenwei Li[a,b], Yu Sun[a,b], Franziska Hess[c], Igor Djerdj[d], Joachim Sann[b], Pascal Voepel[b], Pascal Cop[b], Yanglong Guo[a,*], Bernd M. Smarsly[b,*], Herbert Over[b,*]

[a] Key Laboratory for Advanced Materials, Research Institute of Industrial Catalysis, School of Chemistry and Molecular Engineering, East China University of Science and Technology, Shanghai 200237, PR China
[b] Physikalisch-Chemisches Institut, Justus Liebig University, Heinrich-Buff-Ring 17, 35392 Giessen, Germany
[c] Laboratory of Electrochemical Interfaces, Department of Nuclear Science & Engineering, MIT, 77 Massachuetts Avenue, 13-3034, Cambridge, MA 02139, USA
[d] Department of Chemistry, J. J. Strossmayer University of Osijek, Ulica cara Hadrijana 8/a, HR-31000 Osijek, Croatia

ARTICLE INFO

Keywords:
Deacon process
Stability
CeO_2
Nano-rods
Zr-doping

ABSTRACT

Mixed $Ce_{1-x}Zr_xO_2$ nano-rod particles with varying Zr doping levels of up to 20% were exposed to Deacon reaction mixtures with high HCl concentration at a reaction temperature of 430 °C. The mixed $Ce_{1-x}Zr_xO_2$ nano-rod samples were characterized before and after Deacon reaction by x-ray diffraction (XRD), transmission electron microscopy (TEM), and x-ray photoelectron spectroscopy (XPS). Pure CeO_2 nano-rods are shown to suffer from bulk-chlorination of the catalyst ($CeCl_3x6H_2O$) for reaction mixtures $HCl:O_2 > 2$ that is accompanied by dramatic activity losses. For a reaction mixture of $HCl:O_2 = 2.5:1$, already 5% Zr doping suffices to stabilize the structure $Ce_{1-x}Zr_xO_2$ nano-rods against bulk chlorination. Although $ZrCl_4$ is volatile above 330 °C, we do not encounter discharge of Zr from the fixed bed flow reactor as long as severe bulk chlorination of the $Ce_{1-x}Zr_xO_2$ catalysts in the form of $CeCl_3$ is not observed in XRD. With a simple quasi steady-state model we can corroborate the stabilizing effect of Zr assuming that $ZrCl_4$ evaporation is limited by diffusion of Zr^{4+} in the ceria-zirconia subsurface. As qunatified with XPS the chlorine concentration of stable and active $Ce_{1-x}Zr_xO_2$ nano-rods with 5% Zr is too high to be solely ascribed to on-surface chlorine. The incorporation of Cl into the surface-near region is further supported by XPS experiments performed after oxygen plasma treatment. For even more harsh reaction conditions $HCl:O_2 = 3:1$ none of the $Ce_{1-x}Zr_xO_2$ nano-rods was stable at 430 °C. However, an increase of the reaction temperature to 500 °C enables even pure CeO_2 nano-rods to be stable under such harsh reaction conditions.

1. Introduction

The heterogeneously catalyzed gas-phase oxidation of HCl (Deacon process) is a large-scale and energy-efficient way to recover Cl_2 from gaseous HCl waste [1,2], which is an inevitable by-product from chlorine-related chemical processes such as the industrial synthesis of polyurethanes, polycarbonates, and chlorinated polypropylene. These processes leads to some 10 million tons per year of HCl by-product. Industrial uses do exist for HCl for instance as chlorine source in the polyvinylchloride (PVC) production, as acid catalysts or for the neutralization of alkaline streams. However, chlorine-related processes produce much more of the by-product HCl than the market can absorb, resulting in a severe toxic-waste disposal problem. The primary method of HCl disposal is neutralization that is far from being sustainable since "energetic" HCl gas is transformed into less useful chloride salts. Another option is the recovery of Cl_2 by electrolysis of HCl, that is a quite (electric) energy-consuming process equivalent to some 100.000 t CO_2 emission per year. Consequently, there has been growing interest in the chemical industry to find a cost-effective and environmentally friendly method for recycling chlorine from hydrogen chloride. The heterogeneously catalyzed HCl oxidation (so-called Deacon process) is such a process which allows to design closed process cycles in which chlorine is recycled almost energy-neutral from the byproduct hydrogen chloride.

However, severe stability issues of the catalysts had prevented the industrialization of the Deacon process for 140 years until 1999, when Sumitomo Chemical introduced a catalyst based on RuO_2 supported on rutile-TiO_2, featuring remarkably high activity combined with long-

* Corresponding authors.
E-mail addresses: ylguo@ecust.edu.cn (Y. Guo), Bernd.Smarsly@phys.Chemie.uni-giessen.de (B.M. Smarsly), herbert.over@phys.chemie.uni-giessen.de (H. Over).

https://doi.org/10.1016/j.apcatb.2018.08.047
Received 8 May 2018; Received in revised form 6 August 2018; Accepted 17 August 2018
Available online 19 August 2018

term stability [3]. Nevertheless, the high and fluctuating market price of ruthenium may limit large-scale application of the Sumitomo process, calling for more cost-effective catalysts to replace the RuO_2-based catalysts [4–6].

CeO_2 has been proposed as a promising catalyst material for the HCl oxidation, and it was suggested that the oxygen storage capacity (OSC) and catalytic activity are interrelated [7]. However, CeO_2 suffers from bulk chlorination under harsh reaction condition (i.e. HCl excess) at 430 °C, a typically applied reaction temperature, accompanied by a loss of catalytic activity. Farra et al. found by Prompt Gamma-Ray Activation Analysis (PGAA) that chlorination of CeO_2 is correlated with catalytic activity: the more $CeCl_3$ is formed during the Deacon reaction the lower is the reactivity [8,9]. Recently, it was found that the catalytic stability of pure CeO_2 in the Deacon reaction against chlorination depends sensitively on the exposed facets of the particles. The highest stability against bulk chlorination together with highest activity was encountered with (110) facets preferentially exposed by CeO_2 nano-rods [10].

It is well-documented that incorporating isovalent Zr^{4+} cations into the CeO_2 lattice can strongly facilitate its redox properties and the exchange of oxygen [11–18]. Zr^{4+} doping has also shown to be a feasible strategy to improve the catalytic stability in the Deacon process [8,9,19,20]. For polycrystalline mixed oxide $Ce_{1-x}Zr_xO_2$ nanofibers [19], 20% Zr doping is required to stabilize the fiber structure on the mesoscale, while 10% of Zr suffices already to prevent bulk chlorination according to XRD data. Yet, chemical stabilization by Zr^{4+} is not fully understood since potentially formed $ZrCl_4$ is volatile above 330°C and may leave the reactor for typical reaction conditions of 430°C.

Previously, Zr-doped CeO_2 single-crystalline nano-rods were successfully synthesized for Zr concentrations up to 20% [21] and applied to various catalytic reactions, including styrene epoxidation [22], CO oxidation [23], catalytic reduction of NO [14], and the ethanol-reforming reaction [21]. In order to deepen the microscopic understanding of the stabilizing effect of Zr^{4+}, $Ce_{1-x}Zr_xO_2$ nano-rods (x = 0-0.2) were synthesized by a hydrothermal method and catalytically tested in the Deacon reaction under various reaction conditions, i.e., different ratios of HCl to O_2 in feed gas, and different reaction temperatures. Both oxygen storage capacity (OSC) and complete oxygen storage capacity (OSCc) were evaluated for fresh materials and correlated with the catalytic activity. X-ray diffraction (XRD), X-ray photoelectron spectroscopy (XPS), and transmission electron microscopy (TEM) were employed for the catalyst characterization before and after Deacon reaction in order to study the changes of the nano-rods in terms of crystallinity, composition, and morphology and to correlate them to the catalytic activity. The stabilization of CeO_2 nano-rods by Zr insertion was rationalized by quasi steady state model.

2. Experimental details

$Ce_{1-x}Zr_xO_2$ nano-rods were synthesized by a previously published hydrothermal method [21,24,25]. The general synthesis of mixed oxide nano-rods is exemplified with $Ce_{0.8}Zr_{0.2}O_2$: The mixed Ce/Zr solution (0.8 mmol $Ce(NO_3)_3{\cdot}6H_2O$ (Sigma-Aldrich 99%) + 0.2 mmol $ZrO(NO_3)_3{\cdot}nH_2O$ (Sigma-Aldrich 99%) + 2.5 mL deionized water) was first dripped into a NaOH solution (4.8 *g* NaOH + 17.5 mL deionized water), placed in a Teflon liner (40 ml) and stirred for 30 min. The Teflon liner was then placed inside the autoclave keeping the temperature at 100 °C for 24 h. Next, the precipitates were separated by centrifugation (7000 1/min for 10 min) and subsequently washed by deionized water and ethanol three times separately, followed by drying at 80 °C in air overnight. Finally, the samples were calcined at 600 °C for 6 h in a muffle oven (heating rate of 5 K/min). The calcination temperature of 600 °C was chosen to be high enough to suppress the further temperature-induced sintering of the particles during the Deacon reaction.

Transmission electron microscopy (TEM) was performed on a Philipps CM30 instrument operated at 300 kV. Copper mesh grids were used for the sample preparation. The sample was ultrasonically suspended in ethanol, and one or two droplets of this slurry were deposited on a copper grid.

Structural information of the catalyst was gained by X-ray diffraction (XRD) which was conducted in Θ-2Θ geometry on a Panalytical X'Pert PRO diffractometer with a Cu K_α source (40 kV, 40 mA). Rietveld analysis was carried out by using the FullProf program (Version 2.05).

X-ray photoemission spectroscopy (XPS) experiments (PHI VersaProbe II) were performed with a photon energy of 1486.6 eV (monochromatized Al-K_α line) and an x-ray spot size of ~200 µm with an excitation power of ~50 W to quantify the concentration of Zr, Ce and Cl in the near-surface region of the nano-rod particles. For quantifying the Zr surface concentration the Zr3d spectrum is referenced against the Ce4d rather than to Ce3d spectrum to allow for similar kinetic energies of both emitted photoelectrons (Zr3d, Ce3d). Typical relative error bars for the concentration ratios are 10%. Charging of the sample was compensated by a flow of electrons with energies of about 1 eV and Ar^+ ions of about 10 eV. The survey spectra were taken with an analyzer pass energy of 93.9 eV and a step size of 0.8 eV while the detail spectra were acquired with a pass energy of 23.5 eV and a step size of 0.2 eV. The chamber pressure was ~10^{-6} Pa during the measurement and all spectra were taken at room temperature. The XPS data were analyzed with CasaXPS Version 2.3.17. For some samples a plasma cleaning procedure (GV10x Downstream Asher from ibss Group) was applied by exposing the samples to an air plasma for 20 min. The plasma is created by an inductively coupled RF field (75 W).

The catalytic tests of $Ce_{1-x}Zr_xO_2$ nano-rods were conducted in a fixed bed flow reactor at ambient pressure. The homemade reactor setup [26] includes the gas supply, the quartz tube reactor, heated by the furnace, and the UV/Vis spectrometer for analytic chlorine quantification. The flow of gases, supplied by AirLiquide (HCl 4.5, O_2 4.8 and Ar 5.0), were controlled by digital mass flow controllers (MKS Instruments 1179B). Prior to feeding into the reactor, Ar was dried using a water absorption cartridge (ALPHAGAZ™ purifier H_2O-free, AirLiquide).The reaction temperature was computer-controlled. The product composition was analyzed in a Z-shaped flow cell, combined with a fiber-optic UV–Vis spectrometer (Ocean Optics USB4000 with a DH-2000-BAL light source). The absorbance at a wavelength of λ_{max} = 329 nm (absorption maximum of chlorine) is proportional to the chlorine space time yield (STY) and was quantified by calibration against KI titration. The reaction feeds contained 10 vol.% O_2 and varying HCl concentrations from 20 vol.%, 25 vol.% to 30 vol.% balanced by Ar. The total volumetric flow rate for the reaction was set to 15 $cm^3STPmin^{-1}$ (sccm). For the catalytic tests, typically 20 mg material was supported between quartz wool wads in the reactor tube. The furnace was heated to mostly 430 °C (and 500 °C for one experiment) with a rate of 10 K/min and held for 24 h under reactant stream. The catalyst was only exposed to the O_2 and HCl mixture after the reaction temperature had been reached in Ar atmosphere.

The activity data were normalized to the BET surface area, measured by N_2 physisorption (AUTOSORB-6; Quantachrome, Boynton Beach, USA) at 77 K.

The oxygen storage capacity (OSC) reactor consists of a stainless steel tube (i.d. 4 mm, length 60 mm) connected to the rest of equipment by stainless steel leads (i.d. 1.6 mm) via Swagelok tube fittings [27,28]. The OSC reactor was heated to 430 °C (at the rate of 10 K/min); this temperature was chosen to compare OCS/OCSc with activity data at the same temperature. Carbon monoxide (Praxair, quality 4.7) was used as the reducing agent. Typically, 25 mg catalyst sample was weighted out after drying at 100 °C for 12 h and then loaded into the reactor. The samples were supported between quartz wool wads. To determine the plain oxygen storage capacity (OSC), i.e. the most active oxygen species in the near-surface region of the sample, the stream selector was switched to CO for 2 s (0.067 mL STP of CO), then for 80 s pure Ar was fed, and the stream selector was switched to O_2 for 2 s (0.067 mL STP of O_2).

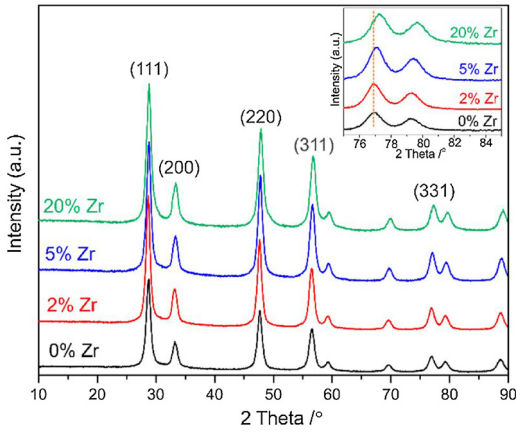

Fig. 1. XRD 2θ scans of the as-prepared $Ce_{1-x}Zr_xO_2$ nano-rods (x = 0 to 0.2). Inset: magnified 2θ-scan around the (331) reflection in order to emphasize the shift of diffraction angle θ to higher values upon Zr incorporation.

The amount of adsorbed oxygen corresponded to the OSC. To determine the complete oxygen storage capacity (OSCc) nine sequential CO pulses of 10 s each (0.33 mL STP of CO each) were applied, separated by 60 s when pure Ar was fed. Subsequently, five 2 s pulses of oxygen were fed, separated by 80 s periods when only Ar was fed. The total amount of oxygen absorbed defines the OSCc that is assumed to approach the oxygen storage capacity of the bulk nano-rod.

3. Results and discussion

3.1. Characterization of the as-prepared catalysts

Fig. 1 presents XRD patterns of freshly prepared $Ce_{1-x}Zr_xO_2$ nano-rods for various Zr concentrations. The observed reflections of all the catalysts belong to the cubic fluorite structure of CeO_2 (JCPDS NO. 34-0394). In none of the samples XRD signals indexed to ZrO_2 are detected, even for doping concentrations of Zr^{4+} reaching 20 mol%, signifying a phase-pure solid solution of $Ce_{1-x}Zr_xO_2$. The (331) signal gradually shifts towards higher diffraction angles with increasing Zr^{4+} concentration (inset of Fig. 1), reflecting the known lattice contraction by Zr incorporation. The lattice parameter values, calculated by Rietveld refinement, are 0.541 nm, 0.541 nm, 0.540 nm, and 0.539 nm (**cf.** Table 1) for CeO_2, $Ce_{0.98}Zr_{0.02}O_2$, $Ce_{0.95}Zr_{0.05}O_2$, and $Ce_{0.8}Zr_{0.2}O_2$, respectively. Similar contractions have been reported for $Ce_{1-x}Zr_xO_2$ powder samples and are summarized in the Vegard plot [29,30]. The observed reduction of the lattice parameter is caused by the lattice contraction induced by the replacement of Ce^{4+} (0.097 nm) by slightly smaller Zr^{4+} (0.084 nm). This finding indicates that Zr is successfully incorporated into the CeO_2 lattice in agreement with previous studies [21]. Simultaneously to the lattice contraction, the incorporation by Zr^{4+} also reduces the average crystalline size, calculated by Rietveld refinement, from 8.5 nm for CeO_2 nano-rods to 6.9 nm for $Ce_{0.8}Zr_{0.2}O_2$ nano-rods (**cf.** Table 1). For polycrystalline $Ce_{1-x}Zr_xO_2$ nanofibers the decrease in particle size was shown to be even more pronounced [19].

Physisorption experiments reveal BET surface areas of 90 m^2/g, 86 m^2/g, 92 m^2/g, and 80 m^2/g for CeO_2, $Ce_{0.98}Zr_{0.02}O_2$, $Ce_{0.95}Zr_{0.05}O_2$, and $Ce_{0.8}Zr_{0.2}O_2$, respectively (**cf.** Table 1). Thus, the BET surface of all studied nano-rod samples is about 86 ± 6 m^2/g, thus allowing for a direct comparison of activity (STY) and OSC data without further normalization to the BET surface area.

Fig. 2 depicts TEM images of the as-prepared $Ce_{1-x}Zr_xO_2$ nano-rods. All of them exhibit a rod-shaped morphology with a mean diameter of 7.5 ± 0.5 nm (**cf. Figure S1**), which is consistent with the crystalline size estimated by Rietveld refinement of XRD data. The average length of the pure CeO_2 nano-rods is around 200 nm. However, with increasing Zr concentration the average length of the nano-rods decreases remarkably to 150 nm, 80 nm and 50 nm for $Ce_{0.98}Zr_{0.02}O_2$, $Ce_{0.95}Zr_{0.05}O_2$, and $Ce_{0.8}Zr_{0.2}O_2$ nano-rods, respectively.

The apparent discrepancy between these TEM-based particle sizes and the average crystallite sizes determined by XRD (ca. 7–10 nm) might have different reasons. First, a particle might consist of several crystallographically different domains along the long particle axis, separated by grain boundaries, which is hardly detectable by our TEM setup. Second, owing to the cubic symmetry one particular reflection in powder XRD is the superposition of formally different reflections (e.g. 11-1, 111, -111, etc.). Hence, the integral width of one XRD reflections provides an average over various reflections and therefore cannot correspond to the length in the direction of the long particle axis.

OSC and OSCc values, representing the ability of oxygen storage/release that is considered to play a key role for the activity of several oxidation reactions, are summarized in Fig. 3. As the Zr content increases from 0% to 20 mol%, the plain oxygen-storage capacity (OSC) keeps almost constant at 63 ± 3 μmol(O)/g (**cf.** Table 1) which may be attributed to the similar BET surface areas and a comparable O vacancy concentration at the surface. Note that the BET surface areas do not change upon the OSC/OSCc experiments, as the applied temperature (430 °C) is substantially lower than the temperature applied in the particle synthesis (600 °C). The found OSC values are in broad agreement with those of a previous study on polycrystalline $Ce_{1-x}Zr_xO_2$ nanofibers [27]. For instance, $Ce_{0.8}Zr_{0.2}O_2$ nanofibers showed an OSC value of 50 μmol(O)/g, while the as-prepared $Ce_{0.8}Zr_{0.2}O_2$ nano-rods, being identical to the ones used in this study, revealed 66 μmol(O)/g for the OSC [27].

Quite in contrast to the OSC, the complete oxygen-storage capacity (OSCc) increases from 188 μmol(O)/g (0%Zr) to 286 μmol(O)/g (2% Zr), and further to 458 μmol(O)/g 5% Zr doping. The trend in OSCc fits quite well to a previous study on mixed nanofibers [19] and other studies from the literature [31,32]. The main reason for the higher OSCc is seen in the lowering of the activation energy for oxygen-ion diffusion and O vacancy formation due to the substitution of Ce^{4+} (0.097 nm) by Zr^{4+} (0.084 nm) [31]. However, the OSCc was improved only very little (472 μmol(O)/g) when Zr doping is further increased to 20%, indicating that already for 5% Zr doping the entire bulk of the particle is participating in the OSCc.

A direct comparison with the activity (Fig. 3) reveals that the STY values of $Ce_{1-x}Zr_xO_2$ nano-rods under mild reaction conditions are practically independent of the Zr concentration, similar to the BET surface and the OSC. We would like to notice that most of the reported OSC values in literatures are actually OSCc values since Ar/H_2 mixture as reduction gas are employed for quite long time periods (minutes)

Table 1
Characterization of the as-prepared $Ce_{1-x}Zr_xO_2$ nano-rods.

	BET surface area ($m^2\,g^{-1}$)	Lattice Parameter (nm)[a]	Crystalline Size (nm)[a]	Surface atomic concentration Zr/(Zr + Ce)[b]	OSC μmol(O)/g	OSCc μmol(O)/g
CeO_2	90	0.541	8.5	0	61	188
$Ce_{0.98}Zr_{0.02}O_2$	86	0.541	8.0	2%	60	288
$Ce_{0.95}Zr_{0.05}O_2$	92	0.540	7.5	3%	61	458
$Ce_{0.8}Zr_{0.2}O_2$	80	0.539	6.9	17%	66	472

a: determined by Rietveld refinement. b: determined by XPS.

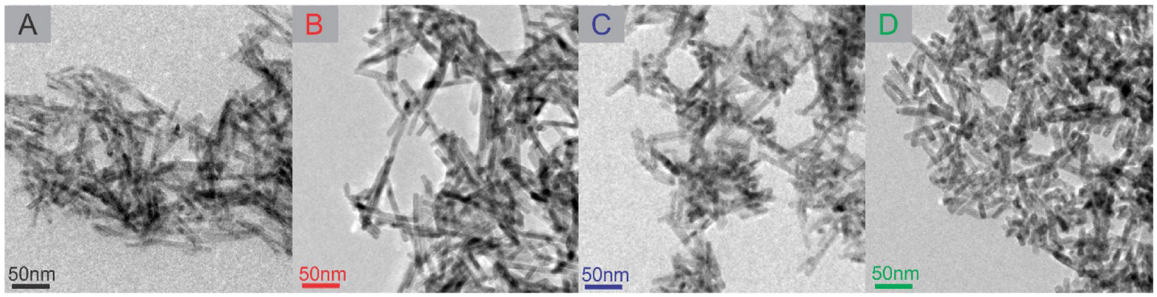

Fig. 2. TEM images of as-prepared $Ce_{1-x}Zr_xO_2$ nano-rods. A): CeO_2, B): $Ce_{0.98}Zr_{0.02}O_2$, C): $Ce_{0.95}Zr_{0.05}O_2$, D): $Ce_{0.8}Zr_{0.2}O_2$.

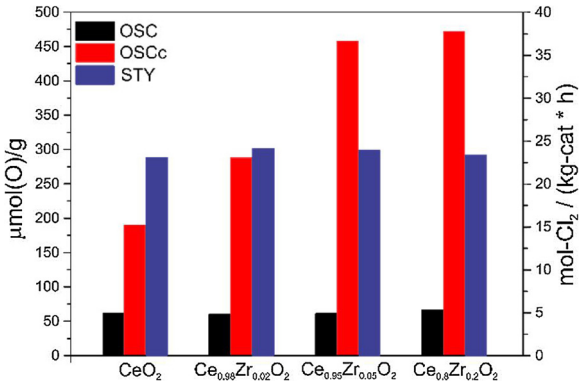

Fig. 3. Plain oxygen-storage capacity, complete oxygen-storage capacity (OSC and OSCc, respectively) of the as-prepared $Ce_{1-x}Zr_xO_2$ nano-rods in comparison with their catalytic activity under mild conditions (Ar:HCl:O_2 = 7:1:2).

rather than short pulses (1–2 s). The published protocols for OSC measurements differ quite substantially among various research studies, thus impairing a direct comparison with literature values. These uncertainties in the OSC/OSCc determination call for harmonization of the experimental procedure.

In order to quantify the concentration of Zr^{4+} in the surface region, we conducted XPS experiments of as-prepared $Ce_{1-x}Zr_xO_2$ nano-rods. From the Zr 3d and Ce 4d spectra shown in **Figure S2** the atomic ratio of Zr/(Zr + Ce) is determined as 0, 2%, 3% and 17% for CeO_2, $Ce_{0.98}Zr_{0.02}O_2$, $Ce_{0.95}Zr_{0.05}O_2$, and $Ce_{0.8}Zr_{0.2}O_2$ respectively, thus being reconciled with the bulk stoichiometries. Obviously, no substantial segregation of surface Zr towards the surface nor dissolution of Zr into the bulk is observed.

3.2. Activity/stability experiment: HCl oxidation reaction

The activity experiments are summarized in Fig. 4. The reactor was heated up to the reaction temperature of 430 °C in pure Ar flow of 15 sccm. Subsequently, the Ar flow was switched to the actual reaction mixture feeds (Ar:HCl:O_2 = 7:2:1 or Ar:HCl:O_2 = 6.5:2.5:1 or Ar:HCl:O_2 = 6:3:1) for 24 h, and the space time yield (STY) was measured online by UV–vis spectroscopy. For a composition of Ar:HCl:O_2 = 7:2:1 (cf. Fig. 4A), pure CeO_2 nano-rods revealed a substantial decrease in activity during the first 5 h on stream, and the activity keeps slowly decreasing during the residual reaction time. Based on XRD experiments we presume that part of CeO_2 suffered from bulk chlorination, i.e. the formation of crystalline $CeCl_3{\cdot}nH_2O$.

Next, $Ce_{0.98}Zr_{0.02}O_2$ nano-rods were exposed to the same reaction condition (430 °C), reaching steady-state of STY after 2 h. These experiments indicated that 2% Zr^{4+} doping was sufficient to maintain catalytic stability of CeO_2 in terms of activity under the reaction condition of Ar:HCl:O_2 = 7:2:1. It was furthermore observed that $Ce_{0.95}Zr_{0.05}O_2$ and $Ce_{0.8}Zr_{0.2}O_2$ nano-rods were also stable under this reaction condition, revealing a comparable activity.

We carried out also activity experiments under even more harsh condition, Ar:HCl:O_2 = 6.5:2.5:1 (cf. Fig. 4B). Obviously, pure CeO_2 nano-rods are unstable, however, the activity curve looks quite different from the one shown in Fig. 4A. The STY decreases continuously during the first 8 h on stream, and the residual activity at steady state is likely due to $CeCl_3{\cdot}nH_2O$, being consistent with the literature [8,33]. For the $Ce_{0.98}Zr_{0.02}O_2$ nano-rods, the activity decreases much more slowly than for pure CeO_2 without reaching steady-state condition even after 24 h, likely due to slow bulk chlorination and morphology alterations (compare XRD experiments in Fig. 5 and TEM experiments in Fig. 6). This result indicates that 2% Zr^{4+} doping is not sufficient to stabilize the Ce-based against bulk chlorination under this harsh reaction condition. Therefore, we additionally measured the activity of $Ce_{0.95}Zr_{0.05}O_2$ and $Ce_{0.8}Zr_{0.2}O_2$ nano-rods under the same reaction condition. Both samples show stable activity and high steady STY with $Ce_{0.8}Zr_{0.2}O_2$ being a little more active than $Ce_{0.95}Zr_{0.05}O_2$. Thus 5% (20%) Zr^{4+} doping cannot only stabilize the Ce-based catalyst against deactivation, but also improves the activity under the harsher reaction condition (Ar:HCl:O_2 = 6.5:2.5:1).

With the purpose of testing the limitation of the improved stability by Zr^{4+} doping, we exposed the $Ce_{1-x}Zr_xO_2$ nano-rods to even harsher reaction condition Ar:HCl:O_2 = 6:3:1 (cf. Fig. 4C). All of the tested

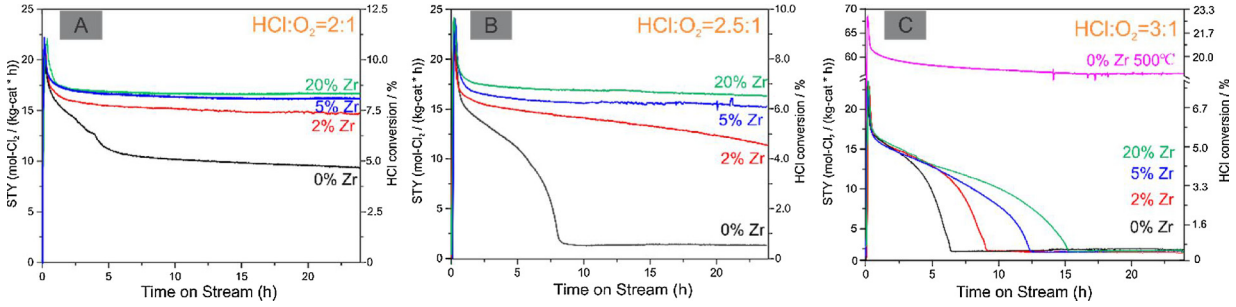

Fig. 4. Space-time yield (STY) per kilogram of catalyst in the HCl oxidation for the $Ce_{1-x}Zr_xO_2$ nano-rods (x = 0.02–0.2). The reaction temperature during the reaction was 430 °C and 500 °C (C, for the CeO_2 sample). A) reaction condition: Ar:HCl:O_2 = 7:2:1, B) reaction condition: Ar:HCl:O_2 = 6.5:2.5:1 and C) reaction condition: Ar:HCl:O_2 = 6:3:1. In all cases, a total flow rate of 15 sccm was applied.

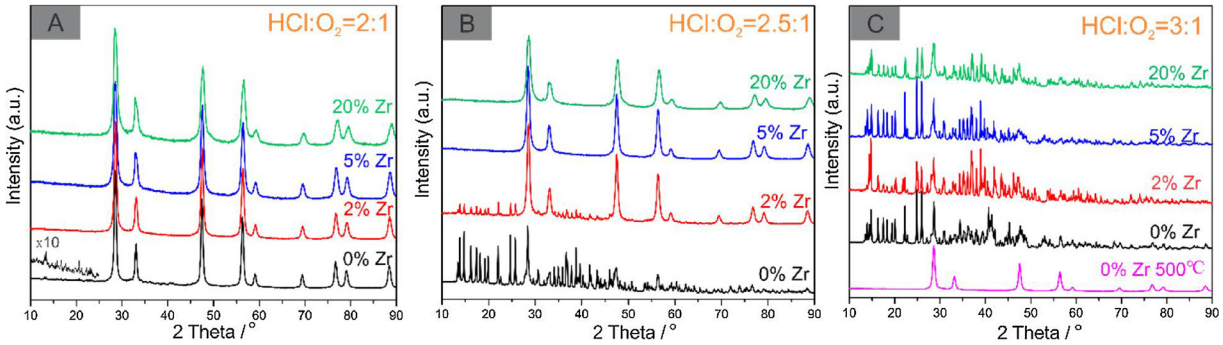

Fig. 5. XRD scans of $Ce_{1-x}Zr_xO_2$ nano-rods after Deacon reaction under different reaction condition. Black: CeO_2, red: $Ce_{0.98}Zr_{0.02}O_2$, blue: $Ce_{0.95}Zr_{0.05}O_2$, green: $Ce_{0.8}Zr_{0.2}O_2$, magenta: CeO_2 under reaction temperature at 500 °C.

catalysts deactivated down to the activity level associated with $CeCl_3{\cdot}nH_2O$. However, the time interval for full deactivation of $Ce_{1-x}Zr_xO_2$ nano-rods strongly depends on the concentration x of doped Zr^{4+}: the higher the initial Zr^{4+} concentration the longer full deactivation takes.

Last, pure CeO_2 nano-rods were exposed to Ar:HCl:O_2 = 6:3:1 reaction mixture, this time however with a higher reaction temperature of 500 °C. Compared to pure CeO_2 nano-rods and reaction temperature of 430 °C, the original STY and steady-state STY is increased by a factor of 3 and 25, respectively, which can be interpreted as thermal activation in terms of the Arrhenius law. Surprisingly, no deactivation is encountered, indicating a stable catalyst under this reaction condition. From these results, we conclude that a higher reaction temperature efficiently improves the stability of pure CeO_2, even under extremely harsh reaction condition, consistent with previously studies [8,33].

The main conclusion drawn from the activity experiments is that besides low HCl concentration (equal to high oxygen concentration) in the feed gas also a high reaction temperature and doping of Zr^{4+} into the CeO_2 nano rod lattice efficiently improve the catalytic stability against deactivation.

3.3. Characterization of $Ce_{1-x}Zr_xO_2$ nano-rods after the catalytic tests

According to our previous study, the stability of CeO_2-based catalysts was directly influenced by bulk chlorination, with the crystalline $CeCl_3{\cdot}nH_2O$ forming during the catalytic reaction [10,33]. In Fig. 5, we present XRD data of $Ce_{1-x}Zr_xO_2$ nano-rods after the Deacon reaction under various conditions for which the activity data are shown in Fig. 4. For the pure CeO_2 nano-rods, $CeCl_3{\cdot}6H_2O$ reflections are detected in XRD for all reaction mixtures, evidencing bulk chlorination and explaining the rapid deactivation of the catalysts. The degree of bulk-chlorination increases with the increasing HCl concentration. For a reaction mixture of Ar:HCl:O_2 = 7:2:1 (430 °C) 2% Zr doping suffices to suppress bulk chlorination (Fig. 5A). For Ar:HCl:O_2 = 6:3:1 at 430 °C all $Ce_{1-x}Zr_xO_2$ nano-rods form massively bulk-chloride after 24 h on stream (Fig. 5C), being fully compatible with the activity data of Fig. 4C.

For gaining a deeper insight into the stabilizing effect of Zr^{4+} doping, reaction-induced changes for Ar:HCl:O_2 = 6.5:2.5:1 at 430 °C (cf. Fig. 4B) are investigated by XRD (Fig. 5B), XPS and TEM (Fig. 6). Under these reaction conditions both pure CeO_2 and $Ce_{0.98}Zr_{0.02}O_2$ suffer from severe bulk-chlorination after 24 h on stream. Quantitative Rietveld refinement of the XRD data reveals that the chlorination degree is strongly dependent on the concentration of Zr^{4+} doping: 70% of pure CeO_2 nano-rods are transformed to $CeCl_3{\cdot}6H_2O$, and the chlorination degree decreases to 11% for $Ce_{0.98}Zr_{0.02}O_2$. Obviously, 2% Zr^{4+} efficiently decreases the chlorination rate, but is unable to fully suppress bulk chlorination. These degrees of bulk-chlorination fit well to the measured near-surface chlorination by XPS (cf. Table 2) with Cl/(Ce + Zr) = 190% and 60% for pure CeO_2 and $Ce_{0.98}Zr_{0.02}O_2$, respectively.

Doping of 5% Zr and 20% Zr both stabilizes CeO_2 nano-rods against bulk chlorination. Nevertheless XPS indicates near-surface chlorination of Cl/(Ce + Zr) = 23% for both $Ce_{0.95}Zr_{0.05}O_2$, and $Ce_{0.8}Zr_{0.2}O_2$ nano-rods. It seems that this surface Cl concentration is self-limiting beyond a Zr^{4+} doping of 5% and is higher than the expected values from on-surface Cl only (about 10%). Quite in contrast to bulk chlorination, surface chlorination is not associated with a loss in catalytic activity (cf. Fig. 4B). However, near-surface chlorination changes the catalytically active phase which is different from the original $Ce_{1-x}Zr_xO_2$ nano-rods with their (110) facets. Besides near-surface chlorination, also the surface Zr concentration slightly increases as revealed by the Zr/(Zr + Ce) ratio of $Ce_{1-x}Zr_xO_2$ nano-rods after the Deacon reaction (cf. Table 2). Perhaps this enrichment of Zr is induced by surface Ce-chloride formation and sublimation.

In order to discriminate between on-surface Cl and Cl in the surface region after the Deacon reaction, we performed the XPS analyses before and after using an air plasma source for cleaning the surface of the nano-rod powders (cf. **Figure S3**). The air plasma removes preferentially adsorbed species. For pure CeO_2 nano-rods after Deacon reaction under Ar:HCl:O_2 = 6:3:1 and a reaction temperature of 500 °C the Cl/Ce ratio is 9.2% that is reduced to Cl/Ce = 0% upon plasma

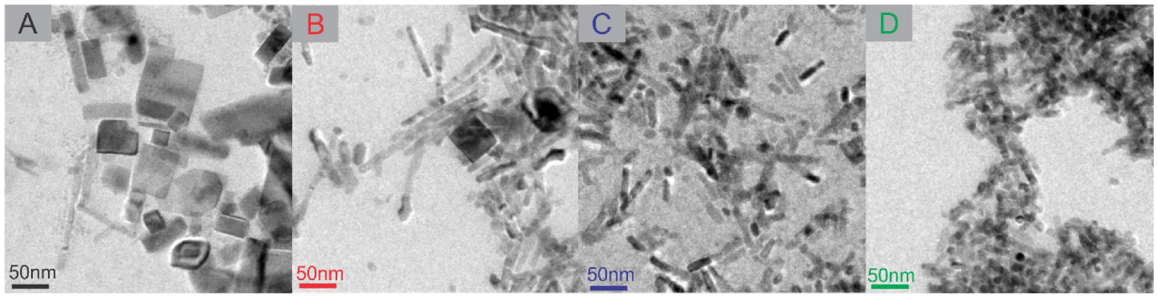

Fig. 6. TEM images of $Ce_{1-x}Zr_xO_2$ nano-rods after the Deacon reaction, performed at 430 °C, with Ar:HCl:O_2 = 6.5:2.5:1. A): CeO_2, B): $Ce_{0.98}Zr_{0.02}O_2$, C): $Ce_{0.95}Zr_{0.05}O_2$, D): $Ce_{0.8}Zr_{0.2}O_2$.

Table 2
Characterization of the $Ce_{1-x}Zr_xO_2$ nano-rods after Deacon reaction under the reaction condition of Ar:HCl:O_2 = 6.5:2.5:1 and a reaction temperature of 430 °C.

	Crystalline Size (nm) [a]	Surface atomic concentration Zr/(Zr + Ce)[b]	Surface atomic concentration Cl/(Ce + Zr)[b]	X $CeCl_3{\cdot}nH_2O$ [a]	Surface atomic concentration Cl/O[b]
CeO_2	15.5&89.3[c]	0	190%	70%	360%
$Ce_{0.98}Zr_{0.02}O_2$	11.1&60.8[c]	2.4%	60%	11%	75%
$Ce_{0.95}Zr_{0.05}O_2$	10.0	4.3%	23%	0	16%
$Ce_{0.8}Zr_{0.2}O_2$	7.2	22.8%	23%	0	17%

a: determined by Rietveld refinement. b: determined by XPS. c: crystalline size of $CeCl_3x6H_2O$. Crystalline Size (nm) were determined by Rietveld refinement for the two different phases.

treatment. This experiment indicates that Cl exists likely only in the form of on-surface Cl on CeO_2 nano-rods. Next we studied the chlorine concentration of $Ce_{0.8}Zr_{0.2}O_2$ nano-rods after Deacon reaction under Ar:HCl:O_2 = 6.5:2.5:1 and a reaction temperature of 430 °C. The Cl/(Ce + Zr) ratio was 22% and reduced to 10% after plasma treatment. From this experiment we infer that a substantial part of the chlorine (about half) is hosted in the surface-near region below the surface. We presume that in all cases (cf. Table 2) where the Cl/(Ce + Zr) concentration is significantly above 10%, Cl is accommodated in the surface-near region below the surface.

For a reaction temperature of 500 °C, XRD (cf. Fig. 5C) indicates that pure CeO_2 nano-rods are stable even under very harsh reaction conditions being consistent with the activity data in Fig. 4C. The average particle size derived from XRD data is 12.7 nm, being significantly larger than the particles size of 8.5 nm for the fresh catalysts. By TEM, one can clearly observe that the nano-rods are still intact, although their width has increased and their length is reduced (cf. **Figure S4**).

Yet, the preservation of the particle shape is particularly interesting: CeO_2 might be indeed stable under these reaction conditions, but the oxidation reaction has to be regarded as a dynamic equilibrium. Thus, the harsh conditions should result in a structural rearrangement and the formation of thermodynamically more stable forms of CeO_2, in particular large crystals. This was not observed in TEM (cf. **Figure S4**), which suggests an intrinsically high stability of such CeO_2 nano-rods with quite small diameters. Further investigations are needed to clarify if indeed the size of the nanoparticles itself does contribute to an enhanced stability in the Deacon reactions.

In order to check for long-term stability we performed also extended catalytic tests over 60 h for the 5% Zr sample on HCl:O_2 = 2.5:1 stream at T = 430 °C (cf. **Figure S5**), indicating that the activity decreases slowly over time with almost constant rate, however without forming an ordered bulk Ce-trichloride as evidenced by post-XRD analysis (cf. **Figure S6**). With this information in mind, we can identify in Fig. 4b,c two stability regions, one where the activity declines linearly and one where the activity drops quite suddenly. Only the latter decline in activity is likely to be associated with the formation of bulk Ce-trichloride.

Nevertheless, in comparison with the pure CeO_2 nano-rods the structural stability of 5% Zr (and 20% Zr) is substantially improved. With XPS (cf. **Table S1**) the Zr concentration is significantly increased after 60 h, indicating that Zr is not discharged from the fixed bed flow reactor but instead the surface is likely depleted of Ce.

In Fig. 6 we summarize the results from TEM characterizations of the $Ce_{1-x}Zr_xO_2$ nano-rods in order to visualize the morphological changes of the sample after Deacon reaction under harsher conditions and 24 h on stream (Ar:HCl:O_2 = 6.5:2.5:1, 430 °C). For pure CeO_2 nano rods dramatic changes are encountered. The rod morphology transforms to cubic or cuboid structure (cf. Fig. 6A). Since most of the CeO_2 is transformed to Ce-chloride (70 mol%), the cuboids in TEM may be assigned to crystalline $CeCl_3{\cdot}6H_2O$ compatible with its space group P2/n. The average particle size of $CeCl_3{\cdot}6H_2O$ in TEM agrees reasonably well with the derived particle size of about 70 nm from XRD. For $Ce_{0.98}Zr_{0.02}O_2$, we can recognize in TEM (cf. Fig. 6B) that the shape of rods is almost not affected, however, the width of the rods is slightly larger with an average value of 10.8 nm (cf. **Figure S7 A**). Also visible in TEM are small cuboids which can be ascribed to the 11% crystalline $CeCl_3{\cdot}nH_2O$ which was derived from the XRD data. For $Ce_{0.95}Zr_{0.05}O_2$, the nano-rods (cf. Fig. 6C), showing an average width of 9.7 nm (cf. **Figure S7 B**), are slightly broader than the fresh ones, but particles with cuboid shape are not observed. Both observations are reconciled with the XRD data (cf. Fig. 5B) that indicate the absence of $CeCl_3{\cdot}6H_2O$ but a slight increase in the particle size. For $Ce_{0.8}Zr_{0.2}O_2$, we cannot observe any morphological alterations in the TEM images (cf. Figs. 6D, 2 D), consistent with the unchanged crystalline size (cf. Tables 1 and 2) and the absence of crystalline $CeCl_3{\cdot}6H_2O$ in the XRD data (cf. Fig. 5B), thus clearly revealing structural stability.

Altogether, we conclude from TEM and XRD that the stability of the $Ce_{1-x}Zr_xO_2$ nano-rods runs in the following order: $Ce_{0.8}Zr_{0.2}O_2$ > $Ce_{0.95}Zr_{0.05}O_2$ > $Ce_{0.98}Zr_{0.02}O_2$ > CeO_2 nano-rods.

From TEM we conclude that the crystalline $CeCl_3x6H_2O$ phase is formed by the growth of separate particles mediated by a mobile precursor species. Exposure of $Ce_{1-x}Zr_xO_2$ nano-rods to a harsh reaction mixture leads to corrosion of the nano-rods and the formation of a mobile molecular $CeCl_3$ species, which in turn nucleates and grows with cuboid shape. This process is particularly evident for pure CeO_2 nano-rods, but is equally observed for $Ce_{0.98}Zr_{0.02}O_2$. For $Ce_{0.98}Zr_{0.02}O_2$ and $Ce_{0.95}Zr_{0.05}O_2$ there is another process evident in TEM, namely the swelling of the nano rods. There are two ways of explanation. Either $CeCl_3{\cdot}6H_2O$ covers the $Ce_{1-x}Zr_xO_2$ nano rods, or chlorine penetrates the surface-near region thereby increasing the layer spacings. Covering of $CeCl_3{\cdot}6H_2O$ would reduce the Zr concentration in XPS that has not been observed experimentally. Therefore, we favor swelling of the nano-rods by chlorine penetration into deeper layers.

In order to clarify the chlorination degree of $Ce_{0.95}Zr_{0.05}O_2$ as a function of reaction time (Ar:HCl:O_2 = 6:3:1 at 430 °C) we took XRD data after 0.5, 2, 4, 8, 12, 16, 24 h on stream (cf. Fig. 7A). The chlorination degree is quantified by Rietveld refinements of the XRD data and presented in Fig. 7B. Below 2 h there is almost no bulk chlorination discernible (induction period), although the activity is decreasing. From 2 h to 18 h, the concentration of $CeCl_3{\cdot}nH_2O$ (chlorination degree) increases steeply from 5% to 79% and finally saturates at 80 ± 1%, while deactivation is now accelerated. This chlorination behavior is reminiscent of a nucleation and growth mode, where during the induction period critical nuclei are formed which subsequently grow further in size until most of the CeO_2 is transformed to $CeCl_3{\cdot}nH_2O$. The activity behavior in Fig. 7b may point to two different deactivation processes, one of them is related to bulk chlorination.

3.4. Thermodynamic considerations of the chlorination process of $Ce_{1-x}Zr_xO_2$ nano-rods

For comparison reasons we determined the Zr concentration of the 20%Zr sample before and after Deacon reaction with HCl:O_2 = 3:1 mixture at 430 °C. Under such conditions the catalyst fully transforms to Ce-bulk chloride, while the Zr concentration substantially decreases from 17% to 6.7% (cf. **Table S1**). This finding reconciles the discharge of Zr from the fixed bed reactor via the thermodynamically favorable $ZrCl_4$ formation and raises questions about the nature of the stabilizing effect of Zr doping observed in our experiments. Even if $Ce_{1-x}Zr_xO_2$ is

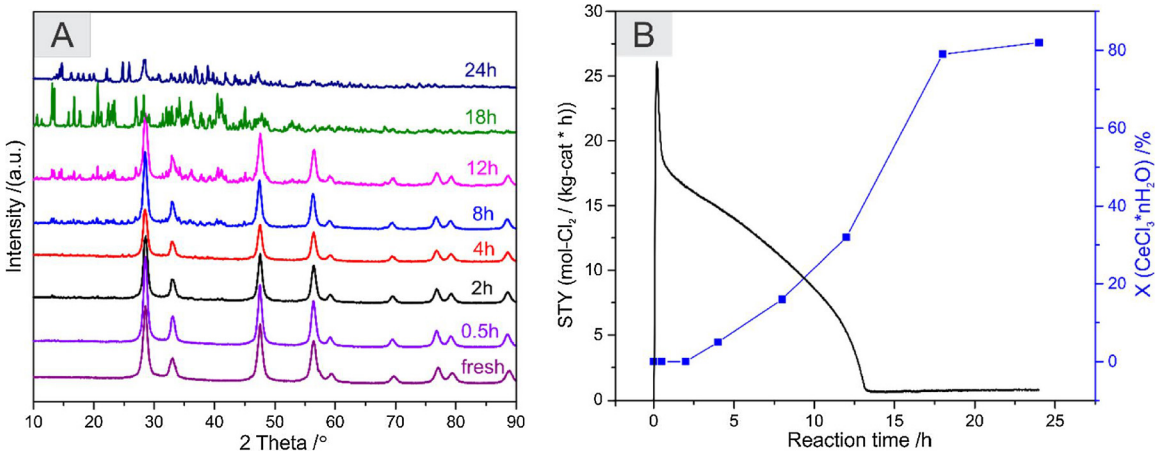

Fig. 7. A): XRD scans of $Ce_{0.95}Zr_{0.05}O_2$ nano-rods after Deacon reaction under reaction condition of Ar:HCl:O_2 = 6:3:1 at 430 °C for different reaction time (from 0 to 24 h). B): chlorination degree x($CeCl_3$·nH_2O) (blue) and STY (black) as a function of reaction time.

less prone to chlorination than pure CeO_2, Zr is not expected to have a long-term stabilizing effect due to irreversible loss of Zr in the form of volatile $ZrCl_4$. Furthermore, ceria-zirconia is well known for forming metastable solid solutions that are prone to segregation and demixing upon annealing [34].

We have shown in a previous contribution that the chlorination of CeO_2 under stationary HCl oxidation conditions can be described in terms of a quasi-stationary approach requiring little more than the thermodynamic data for chlorination as model input [33]. This is the case because the chlorination of CeO_2 is a comparably fast process that can be completed within a few hours and is completely reversible in the sense that reoxidation occurs if the sample is exposed to a sufficiently oxidizing environment [8].

Here, we also modeled the chlorination of $Ce_{1-x}Zr_xO_2$ in a quasi-stationary model based on our previous calculations for pure CeO_2 (details on modeling of $Ce_{1-x}Zr_xO_2$ can be found in **Section S2** of the supporting material). For the ceria-zirconia-related calculations we considered the following two equilibria:

$$R1:\ Ce_{1-x}Zr_xO_2 + 4\,HCl = (1-x)CeCl_3 + x\,ZrCl_4 + 2\,H_2O + (1-x)\frac{1}{2}\,Cl_2$$

$$R3:\ Ce_{1-x}Zr_xO_2 + \left(2x + (1-x)\frac{3}{2}\right)Cl_2 = (1-x)CeCl_3 + x\,ZrCl_{4,gas} + O_2$$

We note that the loss of $ZrCl_4$ cannot be modeled properly in this framework (because every reaction needs a reverse reaction) so that we assume that reoxidation of $ZrCl_4$ is much slower than the chlorination due to negligible partial pressure of $ZrCl_4$ in the gas phase. The steady-state chlorination degree as a function of Zr content calculated according to **Eq. S3** is plotted in Fig. 8 (blue curve). Our model predicts almost total chlorination for pure CeO_2 and $Ce_{1-x}Zr_xO_2$ with more than 35% Zr doping. For the Zr-rich catalysts, this leads to a depletion of ZrO_2. There is a minimum of the chlorination degree at 8% doping, reflecting a more stable regime of the metastable Ceria-Zirconia in the reactive gas atmosphere (cf. **Section S2.2** and **Table S1** in the Supporting material).

In the previous calculation [33], the chlorination (including evaporation of $ZrCl_4$) and dechlorination are described as elementary reactions. However, this approach is clearly insufficient to describe the degradation of our Zr-doped catalyst material because the bulk chlorination comprises a variety of steps, such as adsorption, grain growth, diffusion of cations in the bulk and evaporation of $ZrCl_4$. Particularly the evaporation of $ZrCl_4$ raises questions, because clearly only Zr^{4+} cations located at the surface can form $ZrCl_4$ and evaporate. For progressing degradation Zr^{4+} needs to diffuse to the surface in order to be transformed to $ZrCl_4$. The diffusion coefficient of Zr in Gd-doped CeO_2

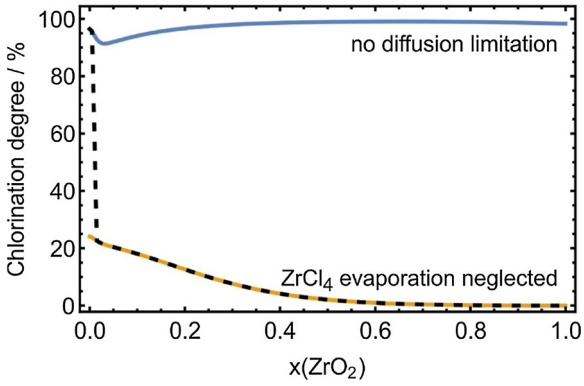

Fig. 8. Chlorination of $Ce_{1-x}Zr_xO_2$ modeled in two steady-state models. The non-diffusion-limited case (blue curve) assumes that $ZrCl_4$ loss is not limited by cation diffusion in the bulk. The diffusion-limited case (orange curve) assumes that $ZrCl_4$ evaporation is limited by cation diffusion and therefore negligible. Experimental results suggest that pure CeO_2 is more appropriately treated in the non-diffusion-limited model, while the diffusion-limited model is more suitable for the doped samples (black dashed curve).

is for instance in the range of 10^{-26} cm^2/s at 700 K [35] when extrapolating from the high-temperature data. Of course, the uncertainty is significant because the Zr diffusion coefficient in $Ce_{1-x}Zr_xO_2$ may differ from the diffusion coefficient in Gd-doped CeO_2 by several orders of magnitude. However, we can assume that the cations in the fluorite structure are practically immobile at the low temperature of our experiment (430 °C). We can thus assume that the deep chlorination of ZrO_2 is completely suppressed on the timescale accessible by our experiment.

To improve our simple steady-state model, we assume therefore that no Zr is exposed at the surface, which allows us to neglect participation of Zr in the chlorination kinetics and all *equilibrium constants* are computed for the respective bulk Zr concentration. We furthermore assume that only the outermost 1 nm of the nanorod is accessible to chlorination, which corresponds to approximately 25% of the total sample volume at a diameter of 7.5 nm. With the chlorination degree computed according to **Eq. S4**, this results in a chlorination curve as shown in Fig. 8 (orange curve). The maximum chlorination degree at low Zr content is 25%, which corresponds to the total chlorination of the outer layer. For increasing Zr content, the chlorination degree decreases, reaching 10% at about 20% Zr doping and then approaches zero.

We recall the massive reconstruction of the pure CeO_2 samples, suggesting that this diffusion-limited model is not applicable to pure CeO_2. We therefore suggest treating pure CeO_2 with the non-diffusion-

limited model and $Ce_{1-x}Zr_xO_2$ with the diffusion-limited model, which is shown in Fig. 8 as black, dashed line. The resulting trend agrees remarkably well with our experimental observation, indicating a chlorination degree for pure CeO_2 is 70% that decreases to 11% for 2% Zr doping.

We note that quantitative agreement should not be expected from this simple modeling (and was not attempted) because the real system is much more complicated in several aspects. A more accurate simulation would require explicit consideration of the precipitation of $CeCl_3{\cdot}nH_2O$ from the ceria-zirconia solid solution and explicit modeling of all elementary reaction steps, including a moving phase boundary as well as gas transport through cracks in the $CeCl_3{\cdot}nH_2O$ surface layer, which is outside the scope of the present work.

4. Conclusion

In the present study solid solutions of $Ce_{1-x}Zr_xO_2$ in the form of nano-rods were successfully synthesized. These $Ce_{1-x}Zr_xO_2$ nano-rods were employed in the Deacon reaction under different reaction condition, namely reaction feed gas composition and temperature. Both activity and stability are shown to be closely related to the HCl to O_2 ratio in the reaction mixture, the reaction temperature and the doping concentration of Zr^{4+}. Excess oxygen in the reaction mixture and doping with Zr^{4+} improve the catalytic stability against bulk chlorination. High reaction temperature increases both catalytic stability and activity.

Pure CeO_2 nano-rods have shown to suffer from bulk-chlorination of the catalyst for all reaction mixtures $HCl:O_2 > 2$ and a reaction temperature of 430 °C that is accompanied by dramatic activity losses. However, for a reaction mixture of $HCl:O_2 = 2.5:1$, already 5% Zr doping suffices to stabilize $Ce_{1-x}Zr_xO_2$ nano-rods against bulk chlorination, i.e., the time for deactivation of the 5% Zr catalyst takes much longer than that of pure CeO_2. From a thermodynamic point of view this result is quite surprising, as Zr in $Ce_{1-x}Zr_xO_2$ nano-rods may form $ZrCl_4$ that is volatile above 330 °C. Therefore, one would expect that Zr is depleted in the near surface region of the $Ce_{1-x}Zr_xO_2$ nano-rods that is clearly not reconciled with XPS experiments. Only after heavy bulk $CeCl_3$ formation has taken place, the Zr concentration decreases substantially according to XPS. The stabilizing effect of Zr was corroborated with a simple quasi steady-state model assuming that $ZrCl_4$ evaporation is limited by diffusion of Zr^{4+} in the ceria-zirconia subsurface.

For even more harsh reaction conditions $HCl:O_2 = 3:1$ none of the $Ce_{1-x}Zr_xO_2$ nano-rods were stable at a reaction temperature of 430 °C. Increasing the reaction temperature to 500 °C enables even pure CeO_2 nano-rods to be stable under such harsh reaction conditions.

The corrosion process of $Ce_{1-x}Zr_xO_2$ nano-rods via bulk-chlorination destroys the nano-rod structure (TEM) and leads to the formation of crystalline $CeCl_3x6H_2O$ with low catalytic activity (TEM, XRD). This bulk-chlorination process proceeds via nucleation and growth, as suggested by TEM and XRD, which is likely to be mediated by a mobile molecular precursor species such as $CeCl_3$. However, even bulk stable $Ce_{1-x}Zr_xO_2$ catalysts reveal enhanced surface chlorination (XPS) and an increase in the diameter of the nano-rods (TEM, XRD). Utilizing oxygen plasma treatment, Cl2p XPS provides evidence for chlorine incorporation into deeper layers in the near surface region of $Ce_{1-x}Zr_xO_2$. The surface chlorine enriched $Ce_{1-x}Zr_xO_2$ may therefore be considered as the catalytically active phase in the Deacon reaction.

Acknowledgments

This work was supported by the National Key Research and Development Program of China (2016YFC0204300), National Natural Science Foundation of China (21577035), Commission of Science and Technology of Shanghai Municipality (13521103402, 15DZ1205305) and 111 Project (B08021). Chenwei Li gratefully acknowledges theChina Scholarship Council for the Joint-Ph.D program between the China Scholarship Council and the Physikalisch-Chemisches Institut of the Justus-Liebig-University Giessen. We would like to thank the Center of Materials Research (LaMa) at Justus Liebig University Giessen for the support of this project.

Appendix A. Supplementary data

Supplementary material related to this article can be found, in the online version, at doi:https://doi.org/10.1016/j.apcatb.2018.08.047.

References

[1] M.W.M. Hisham, S.W. Benson, J. Phys. Chem. 99 (1995) 6194–6198.
[2] J. Perez-Ramirez, C. Mondelli, T. Schmidt, O.F.K. Schlüter, A. Wolf, L. Mleczko, T. Dreier, Energy Environ. Sci. 4 (2011) 4786–4799.
[3] K. Seki, Catal. Surv. Asia 14 (2010) 168–175.
[4] M. Hammes, M. Valtchev, M.B. Roth, K. Stöwe, W.F. Maier, Appl. Catal. B: Environ 131–133 (2013) 389–400.
[5] H. Over, R. Schomäcker, ACS Catal. 3 (2013) 1034–1046.
[6] K.K. Feng, C.W. Li, Y.L. Guo, W.C. Zhan, B.Q. Ma, B.W. Chen, M.Q. Yuan, G.Z. Lu, Appl. Catal. B: Environ 164 (2015) 483–487.
[7] A.P. Amrute, C. Mondelli, M. Moser, G. Novell-Leruth, N. López, D. Rosenthal, R. Farra, M.E. Schuster, D. Schuster, T. Schmidt, J. Pérez-Ramírez, J. Catal. 286 (2012) 287–297.
[8] R. Farra, M. Eichelbaum, R. Schlögl, L. Szentmiklósi, T. Schmidt, A.P. Amrute, C. Mondelli, J. Pérez-Ramírez, D. Teschner, J. Catal. 297 (2013) 119–127.
[9] R. Farra, M. Garcia-Melchor, M. Eichelbaum, M. Hashagen, W. Frandsen, J. Allan, F. Girgsdies, L. Szentmiklósi, N. Lopez, D. Teschner, ACS Catal. 3 (2013) 2256–2268.
[10] C.W. Li, Y. Sun, I. Djerdj, P. Voepel, C. Sack, T. Weller, R. Ellinghaus, J. Sann, Y.L. Guo, B. Smarsly, H. Over, ACS Catal. 7 (2017) 6453–6463.
[11] E. Aneggi, C. Leitenburg, J. Llorca, A. Trovarelli, Catal. Tod. 197 (2012) 119–126.
[12] T. Montini, M. Melchionna, M. Monai, P. Fornasiero, Chem. Rev. 116 (2016) 5987–6041 and references therein.
[13] I. Atribak, A. Bueno-López, A. García-García, J. Catal. 259 (2008) 123–132.
[14] P. Maitarad, D.S. Zhang, R.H. Gao, L.Y. Shi, H.R. Li, L. Huang, T. Rungrotmongkol, J.P. Zhang, J. Phys. Chem. C. 117 (2013) 9999–10006.
[15] L.P. Dos Santos Xavier, V. Rico-Pérez, A.M. Hernández-Giménez, D. Lozano-Castelló, Agustín Bueno-López, Appl. Catal. B: Environ 162 (2015) 412–419.
[16] W. Ruettinger, X. Liu, R.J. Farrauto, Appl. Catal. B: Environ. 65 (2006) 135–141.
[17] M. Yashima, Catal. Today 253 (2015) 3–19.
[18] A. Trovarelli, P. Fornasiero (Eds.), Catalysis by Ceria and Related Materials, 2nd ed., Imperical College Press, London, 2013and references therein.
[19] S. Urban, N. Tarabanko, C.H. Kanzler, K. Zalewska-Wierzbicka, R. Ellinghaus, S.F. Rohrlack, L. Chen, P.J. Klar, B.M. Smarsly, H. Over, Catal Lett. 143 (2013) 1362–1367.
[20] Z.Y. Fei, X.X. Xie, Y. Dai, H.Y. Liu, X. Chen, J.H. Tang, M.F. Cui, X. Qiao, Ind. Eng. Chem. Res. 53 (2014) 19438–19445.
[21] W. Chen, K. Chen, M. Wang, S. Weng, C. Lee, M.C. Lin, Chem. Commun. 46 (2010) 3286–3288.
[22] X. Liu, J. Ding, X. Lin, R.H. Gao, Z.H. Li, W.L. Dai, Appl. Catal. A: General 503 (2015) 117–123.
[23] A. Chen, Y. Zhou, N. Ta, Y. Li, W.S. Shen, Catal. Sci. Technol. 5 (2015) 4184–4192.
[24] H. Mai, L. Sun, Y. Zhang, R. Si, W. Feng, H. Zhang, H. Liu, C. Yan, J. Phys. Chem. B. 109 (2005) 24380–24385.
[25] J. He, T. Xu, Z. Wang, Q. Zhang, W. Deng, Y. Wang, Angew. Chem. Int. Ed. 51 (2012) 2438–2442.
[26] Ch. Kanzler, S. Urban, K. Zalewska-Wierzbicka, F. Hess, S.F. Rohrlack, C. Wessel, R. Ostermann, J.P. Hofmann, B.M. Smarsly, H. Over, Chem Cat. Chem. 5 (2013) 2621–2626.
[27] M. Möller, H. Over, B. Smarsly, N. Tarabanko, S. Urban, Catal. Today 253 (2015) 2017–2218.
[28] M. Möller, S. Urban, P. Cop, T. Weller, R. Ellinghaus, M. Kleine-Boymann, C. Fiedler, J. Sann, J. Janek, L. Chen, P.J. Klar, D.M. Hofmann, J. Philipps, P. Dolcet, S. Gross, H. Over, B.M. Smarsly, Chem. Catal. Chem 7 (2015) 3738–3747.
[29] W.T. Gibbons, L.J. Venstrom, R.M. De Smith, J.H. Davidson, G.S. Jackson, Phys. Chem. Chem. Phys. 16 (2014) 14271–14280.
[30] M. Epifani, T. Andreu, S. Abdollahzadeh-Ghom, J. Arbiol, J. Morante, Adv. Funct. Mater. 22 (2012) 2867–2875.
[31] A. Trovarelli, F. Zamar, J. Llorca, C. Leitenburg, G. Dolcetti, J.T. Kiss, J. Catal. 169 (1997) 490–502.
[32] P. Fornasiero, R. Di Monte, G. Ranga Rao, J. Kaspar, S. Meriani, A. Trovarelli, M. Graziani, J. Catal. 151 (1995) 168–177.
[33] C.W. Li, F. Hess, I. Djerdj, G.T. Chai, Y. Sun, Y.L. Guo, B. Smarsly, H. Over, J. Catal. 357 (2018) 257–262.
[34] R. Grau-Crespo, N.H. de Leeuw, S. Hamad, U.V. Waghmare, Proc. R. Soc. 468 (2011) 1925–1938 and references therein.
[35] S. Beschnitt, R.A. De Souza, Solid State Ion. 305 (2017) 23029.